Journal of Cleaner Production 485 (2024) 144378

Contents lists available at ScienceDirect

Journal of Cleaner Production

journal homepage: www.elsevier.com/locate/jclepro

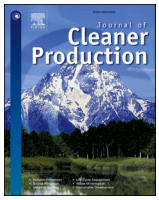

Development of a multi-objective support tool for optimizing phosphorus recovery from sewage sludge ash: A step towards process feasibility

Lorenzo Esposito [a], Gaia Boniardi [a], Marco Frigerio [b], Maitane Guembe [c], Íñigo X. García-Zubiri [c], Daniel El Chami [d], Roberto Canziani [a], Andrea Turolla [a,*]

[a] Politecnico di Milano, Department of Civil and Environmental Engineering (DICA) – Environmental Section, Piazza Leonardo da Vinci 32, 20133, Milano, Italy
[b] SEAM Engineering – Via Cavour 2, 22074, Lomazzo, CO, Italy
[c] MAGNA – Magnesitas Navarras S.A., Av. Roncesvalles s/n, 31630, Zubiri, Navarre, Spain
[d] TIMAC AGRO Italia S.p.A., S.P.13 – Località Ca' Nova, 26010, Ripalta Arpina, CR, Italy

ARTICLE INFO

Handling Editor: Mingzhou Jin

Keywords:
Bio-based fertilizers
Design of experiments
Economic feasibility
Integrated assessment
Process optimization
Wet acid leaching

ABSTRACT

Phosphorus (P) recovery from Sewage Sludge Ash (SSA) represents a promising solution to P supply concerns, with the main application challenge consisting of the poor economic feasibility of current technologies, requiring Operating Expense (OPEX) reduction to compete with primary P sources. This study aims to provide a multi-objective support tool for the design and operation of P recovery from SSA by combined wet acid leaching and alkaline precipitation to produce bio-based fertilizers. First, in the view of filling literature gaps, lab-scale leaching tests based on the Design of Experiment were performed with SSA from a full-scale mono-incinerator, and multi-variate statistical techniques were applied to generate polynomial regression models for Mg, K, Cu and Zn extraction. Then, small pilot-scale leaching and precipitation tests were conducted, applying HCl and H_2SO_4 as leaching agents and $Ca(OH)_2$ and a low-grade magnesium oxide mining by-product (LG-MgO) as precipitating agents. Lab- and pilot-scale data were then jointly employed to develop the support tool that was later applied for process optimization based on a set of key performance indicators. The support tool indicated the optimal leaching (HCl, 0.82 N, 10 L/kg, 0.5 h) and precipitation ($Ca(OH)_2$) operating parameters for obtaining EU-compliant fertilizing products while minimizing OPEX in different pricing scenarios. Furthermore, as chemical supply and process solid residue disposal resulted as the most impacting cost items, priority actions for targeting the break-even point were identified.

1. Introduction

Phosphorus (P) plays a pivotal role in sustaining life on earth and human society. Nowadays, around 89% of the worldwide production of P is dedicated to agricultural applications, principally for fertilizers manufacturing (Desmidt et al., 2015; Meng et al., 2019). However, the persistent and increasing P demand is facing various challenges due to a gradual depletion of phosphate rock reserves, their decreasing quality, and their uneven distribution around the world. In addition, the over-application of P-based fertilizers is leading to increasing eutrophication of water bodies. Therefore, recovering P from alternative sources has become crucial to meet the future demand and face rising challenges.

Among the various secondary P sources, wastewater treatment streams (aqueous phases, sewage sludge - SS - and sewage sludge ash - SSA) are the most exploited through existing recovery technologies. Specifically, SSA is considered the most promising one due to its high P content (4–15.7%) comparable with medium-low grade phosphate rocks (5–13%) (Meng et al., 2019; Ryszko et al., 2023; Liu et al., 2021; Fang et al., 2018a; Fang et al., 2021; shan Li et al., 2018; Boniardi et al., 2024a; Worwąg, 2018; Luyckx and Van Caneghem, 2021). However, the high heavy metal concentrations and the low P bioavailability in SSA limit its direct application as a fertilizer, requiring the implementation of P recovery processes (Gorazda et al., 2016; heng Fei et al., 2019; Liang et al., 2019).

Among the different existing P recovery processes from SSA, wet chemical leaching and thermochemical treatment are the most frequently discussed in the literature, with the former being generally preferred based on its effectiveness, flexibility and similarity to the current methods for extracting P from phosphate rocks (Meng et al., 2019; Liu et al., 2021; Fang et al., 2018a, 2021; Luyckx et al., 2020a; Canziani et al., 2023). In particular, several technologies based on wet

* Corresponding author.
E-mail address: andrea.turolla@polimi.it (A. Turolla).

https://doi.org/10.1016/j.jclepro.2024.144378
Received 6 August 2024; Received in revised form 16 November 2024; Accepted 1 December 2024
Available online 2 December 2024

Abbreviations

P = Phosphorus
SS = Sewage Sludge
SSA = Sewage Sludge Ash
EE = Extraction Efficiency
PE = Precipitation Efficiency
Cn = acid concentration
L/S = liquid-to-solid ratio
t = contact time
DoE = Design of Experiment
DoE#1 = full-factorial Design of Experiment
DoE#2 = extended full-factorial Design of Experiment
LG-MgO = low-grade magnesium oxide mining by-product
sol_{ash} = fraction of solubilized ash
ASR = Acid Solid Residue
dm = dry matter content
C_{TSS} = total suspended solids concentration
OPEX = Operating Expense
$\eta_{recovery}$ = Phosphorous recovery efficiency
$ACID_c$ = Commercial-grade acid consumption
ASR_f = Acidic Solid Residues formation
PNT_c = Dry precipitant consumption
$P_{precipitate}$ = Phosphorous content in the precipitate
COMPL = Compliance to EU 2019/1009
P_{rec} = total phosphorus recovered
d_i = individual desirability functions
D = Composite desirability function
BASE = baseline scenario
LP = low-price scenario
HP = high-price scenario

chemical leaching process are going to be implemented at the full-scale in the next decade (each installation treating approximately 20–30 ktonne $_{SSA}$/y), as Ash2Phos (Easy Mining), Ecophos (Prayon), TetraPhos (Remondis), Phos4Green (Glatt), Phos4Life (ZAR – Técnicas Reunidas) and SusPhos (ESPP). Despite that, the economic feasibility of these solutions is still the main challenge to overcome (Li et al., 2019; Xu et al., 2023). In detail, the technologies based on wet chemical processes are usually characterized by Operating Expense (OPEX) between 5 and 6 €/kg P_{rec} (total phosphorus recovered), which are significantly higher than the average price for phosphate rocks (1.1 €/kg P) and for conventional P-based fertilizer (triple superphosphate, 2.2 €/kg P) (IndexMundia; IndexMundib; Egle et al., 2016). Therefore, process intensification and optimization are needed to decrease the OPEX of these alternatives in the view of making the recovered product competitive with current P sources.

Existing literature on optimizing wet chemical P recovery from SSA mostly focuses on the extraction phase, typically evaluated at the lab-scale (Fang et al., 2018a; Liang et al., 2019; Luyckx et al., 2020a; He et al., 2020; Wang et al., 2018; Gorazda et al., 2017; Kootstra et al., 2019; Liu and Qu, 2016; Boniardi et al., 2024b). These studies explored a variety of leaching agents, comprising inorganic acids (H_2SO_4, HCl, HNO_3), organic acids (acetic, citric, formic, gluconic, oxalic), alkaline (NaOH, CaO) and chelating agents (Ethylenediaminetetra acetic acid (EDTA), Nitrilotriacetic acid (NTA), Ethylenediaminetetramethylene phosphonate (EDTMP)). Generally, H_2SO_4 provided the lowest leaching agent costs per kg P extracted, while oxalic acid minimized the heavy metals co-extraction, thus reducing downstream processing costs (Luyckx et al., 2020a; Kootstra et al., 2019). Most of these studies relied on a "one-variable-at-a-time" approach to investigate P and metals/heavy metals/metalloids extraction efficiency (EE), individually assessing the impact of main leaching operating parameters discussed in literature: acid type and concentration (Cn), liquid-to-solid ratio (L/S) and contact time (t) (Meng et al., 2019; Ryszko et al., 2023; Liu et al., 2021; Fang et al., 2021; Gorazda et al., 2016; Liang et al., 2019; Luyckx et al., 2020a; Wang et al., 2018; Liu and Qu, 2016; Boniardi et al., 2021, 2022). Only a few works applied statistical multivariate models to jointly investigate these parameters (Luyckx et al., 2020a; Boniardi et al., 2024b), identifying optimal leaching operating conditions to enhance technical (P EE, kg of P extracted per L of leaching agent per day) and economic (cost of leaching agent per kg of P extracted) indexes. Specifically, different optimal leaching configurations were found based on the SSA alkalinity, with Ca-rich SSA requiring higher Cn and t to achieve P EE > 80% (Boniardi et al., 2024b).

However, to the best of the authors' knowledge, no studies comprehensively assessed the overall techno-economic performance of the P recovery process from SSA by jointly considering the extraction and precipitation phases. Moreover, almost all the existing studies are based on lab-scale experiments, with only one work addressing P recovery at a relevant scale (Boniardi et al., 2024c). Building upon these gaps, this research aims to optimize the P recovery process from SSA based on combined wet acid leaching and alkaline precipitation, assessing the whole process performance via a multi-objective approach. In detail, a support tool for the integrated simulation of the P recovery process from SSA was developed, simultaneously assessing the influence of extraction and precipitation operating parameters on relevant key performance indicators (KPIs) targeted at both the recovery process and the recovered product. Such tool was calibrated by jointly employing data from literature and targeted lab- and pilot-scale experiments.

Lab-scale input data were derived from leaching experiments conducted on SSA from the Werdhölzli full-scale mono-incinerator (Zurich, Switzerland) using the Design of Experiment (DoE) statistical approach. Multi-variate statistical techniques were applied to develop polynomial regression models for Mg, K, Cu and Zn EE, integrating the obtained models with those for P, Al, Ca and Fe EE reported in (Boniardi et al., 2024b) to comprehensively describe the P recovery process as a multi-component system. Pilot-scale input data were derived from leaching and precipitation experiments using HCl and H_2SO_4 as leaching agents and $Ca(OH)_2$ and a low-grade magnesium oxide mining by-product (LG-MgO) as precipitating agents.

The present work aims to advance the current state of art by providing a comprehensive support tool that could help researchers and industry stakeholders to identify optimal process operating conditions and implementation strategies, thus paving the way for further activities to guarantee the overall techno-economic feasibility of the process.

2. Materials and methods

2.1. Support tool

2.1.1. Modelling framework

The support tool was developed to simulate the P recovery process from SSA shown in Fig. 1. The tool enabled the process integrated assessment, identifying proper leaching (acid type, Cn, L/S and t) and precipitation (precipitant type) operating conditions to optimize process performance in terms of relevant KPIs. It consisted of a Microsoft Excel file based on mass balance equations applied to parameters listed in Table 1.

The present work used fly ash sampled from the electro-filters of the Werdhölzli mono-incineration full-scale plant (Zurich, Switzerland) as target SSA. The plant burns around 100,000 tonne/y of dewatered SS from the Zürich canton's wastewater treatment plants in a fluidized bed kiln. Table S1 in SM provides the input treated SSA mass flow rate,

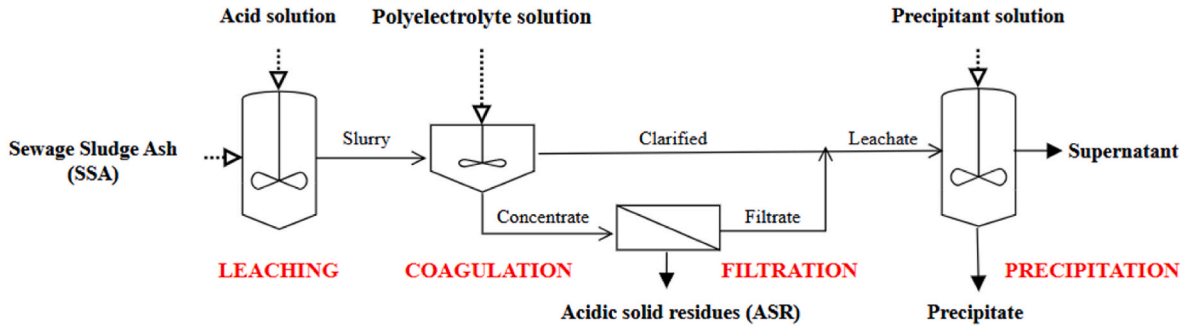

Fig. 1. P recovery process from SSA simulated in the support tool.

Table 1
Mass balance parameters for the P recovery process from SSA simulated in the support tool. "X": element of interest (Al, Ca, Fe, P, Mg, K, Cu, Zn).

Volumetric flow rate	Q	[m^3/h]
Mass flow rate	M	[kg/h]
Density	ρ	[kg/m^3]
Dry matter content	dm	[%]
Total Suspended Solids	TSS	[kg/h], [mg/L]
Total Dissolved Solids	TDS	[kg/h], [mg/L]
Sulphate ion	SO_4^{2-}	[kg/h], [mg/L]
Chloride ion	Cl^-	[kg/h], [mg/L]
Dissolved X	X diss	[kg/h], [mg/L]
Particulate X	X part	[kg/h], [mg/L]

density and elemental composition (Al, Ca, Fe, P, Mg, K, As, Cd, Cr, Hg, Ni, Pb, Cu, Zn), the latter quantitatively determined by aqua regia digestion followed by ICP-AES analysis, according to UNI EN 13657:2004 and EPA 6010D 2018 methods.

A more detailed physical and chemical characterization of the employed SSA (Ash#2) is reported in (Boniardi et al., 2024b). The mass flowrate of SSA was derived from a study carried out by Politecnico di Milano and Gruppo CAP, the water utility responsible for the Integrated Water Service of the Milan metropolitan area. The study aimed to develop a P recovery scenario from the SSA generated by the upcoming mono-incinerator of Sesto San Giovanni (MI, Italy). High-purity H_2SO_4 (96% w/w) and HCl (37% w/w) were selected as commercial-grade acid extractants, while leaching operating ranges were set according to the lab-scale experiments described in subsection 2.2.1.

The simulated leaching phase is based on two key parameters, namely the extraction efficiency (EE) and the fraction of solubilized ash (sol_{ash}), being the latter defined as reported in **Eq. (1)**:

$$sol_{ash}(\%) = \left(1 - \frac{M_{ASR}}{M_{in}}\right) \bullet 100 \qquad \text{Eq. 1}$$

where M_{ASR} is the mass of dried acid solid residue (ASR) and M_{in} is the initial mass of SSA treated.

Al, Ca, Fe and P EE were derived from literature (Boniardi et al., 2024b) (Ash#2, DoE#4), while Mg, K, Cu and Zn EE were individually derived through later-detailed polynomial regression models (subsection 2.2.1). The values for sol_{ash} were set to 13% (H_2SO_4) and 49% (HCl) based on lab-scale findings. Such difference could be attributed to the lower solubility of gypsum compared to calcium chloride, which form respectively when leaching by H_2SO_4 and HCl. Further details on the formation of these salts are reported in (Fang et al., 2018a; He et al., 2020; Liang et al., 2021).

To promote the aggregation of solid ash particles after leaching, a coagulant (i.e., anionic polyelectrolyte solution - 0.2% w/v) was added, whose dosage was based on lab-scale coagulation tests conducted by Tecnoidea Impianti S.r.l. (Villasanta, Italy) on the slurry generated from the leaching of 200 g of SSA under specific leaching conditions (H_2SO_4, 1 N, 10 L/kg, 2 h). The simulated coagulation phase relies on two key parameters, namely the dry matter content (dm) of concentrate and ASR streams, while the filtration depends on the total suspended solids concentration (C_{TSS}) of clarified and filtrate streams (Table S2, SM). Data for concentrate and clarified streams were taken from the above-mentioned coagulation tests, assuming their outcomes were valid for both the acids, while data for ASR and filtrate streams were derived from pilot-scale findings reported in (Boniardi et al., 2024c). The dosage of polyelectrolyte solution was determined by proportionally scaling the corresponding pilot-scale dosage (Table S3, SM) to the volume of acid solution estimated in the mass balance.

As precipitants, alkaline solutions of $Ca(OH)_2$ (30% w/v, 1280 kg/m^3) and LG-MgO (80% w/v, 960 kg/m^3) were adopted, in line with pilot-scale procedures. LG-MgO is a low-grade calcined magnesia by-product provided by the private mining company Magnesitas Navarras (Navarre, Spain). The material consists in the dust/powder collected from the cyclones in the flue gas treatment line of the $MgCO_3$ calcination process. Previous applications of this material are reported in (Erro et al., 2023; Aguilar-Pozo et al., 2023).

The key factor affecting the simulated precipitation phase is the precipitation efficiency (PE), whose values were obtained from pilot-scale findings. Those values served as benchmark for precipitation, independently from the employed leaching operating conditions. The dosage of precipitant solution was calculated by proportionally scaling the corresponding pilot-scale dosage (Table S3, SM) to the volume of leachate estimated in the mass balance. No solid-liquid separation was simulated after the precipitation phase, assuming that the dry precipitant completely solubilizes, the recovered precipitate gets completely

Table 2
KPIs of the P recovery process from SSA reproduced in the support tool. "P_{rec}" is the total phosphorus recovered, thus the phosphorus contained in the precipitate.

Class	Parameter	Abbreviation	U.M.
Recovery process	Operating Expense	OPEX	[€/kg P_{rec}]
	Phosphorous recovery efficiency	$\eta_{recovery}$	[%]
	Commercial-grade acid consumption	$ACID_c$	[kg/kg P_{rec}]
	Acidic Solid Residues formation	ASR_f	[kg/kg P_{rec}]
	Dry precipitant consumption	PNT_c	[kg/kg P_{rec}]
Recovered product	Phosphorous content in the precipitate	$P_{precipitate}$	[%P]
	Compliance to EU 2019/1009	COMPL	[-]

dry, and the supernatant is free of total suspended solids.

2.1.2. KPIs identification

Table 2 displays the KPIs identified for the recovery process and the recovered product. OPEX was calculated based on the unitary prices outlined in Table S4 in SM, most of which were derived from a market survey conducted by the engineering firm SEAM Engineering S.r.l. These cost data are comparable with those available in literature (Luyckx et al., 2020a; Egle et al., 2016; Kootstra et al., 2019; Uzkurt Kaljunen et al., 2022), which can offer a broader context for cost variability. Tap water cost was taken from the price list for business use provided by Gruppo CAP (Gruppo CAP). LG-MgO price was set to 0 €/tonne, excluding possible transport and management costs. Energy requirements were assessed based on estimates from SEAM Engineering S.r.l. in terms of power and number of required devices (Table S5, SM) and working hours per year (7000 h/y). The equipment for solid-liquid separation was accounted for twice, excluding the polyelectrolyte solution preparator, as it is expected to be used after the precipitation stage in a full-scale plant. Phosphorous recovery efficiency ($\eta_{recovery}$) was calculated as the product between P EE and P PE. ASR formation (ASR_f) refers to the wet material, considering its water content. The compliance of recovered products to European regulation on fertilizers (EU, 2019/1009 - Product Function Category 1-C-I, Inorganic macronutrient fertiliser) was quantified as in **Eq. (2)**,

$$COMPL = \sum_{i=1}^{n} \frac{C_i}{C_{i,max}} \Big/ n \quad \text{Eq. 2}$$

where C_i and $C_{i,max}$ are the observed and maximum allowed concentrations of a given element in the recovered product, respectively, and n is the number of elements considered. If COMPL $\geq$1, the precipitate is not compliant with the regulation.

2.1.3. Multi-objective optimization

The multi-objective optimization of the P recovery process was performed by applying the desirability method. This method allows to identify the combination of variable settings that jointly optimize multiple responses, integrating them into a single measure of desirability. The method was selected based on previous studies (Luyckx et al., 2020a; Guedri et al., 2023; Diego Pimenta et al., 2018), which highlighted its higher flexibility with respect to other conventional methods like the Response Surface Methodology. In details, each response was converted into individual desirability functions d_i (0–1), as quantified by **Eq. (3)** and **Eq. (4)**. The former was employed to maximize the specific responses ($P_{precipitate}$, $\eta_{recovery}$), while the latter to minimize them (OPEX, COMPL, $ACID_c$, ASR_f, PNT_c). Target values (Ti) of the i^{th} response were set to the respective individual optimum, while L_i and H_i were set to the respective lowest and highest values assumed. Individual desirability functions were combined into a composite function D (0–1), calculated through a geometric mean (**Eq. (5)**). y_i and w_i are the predicted value and the importance of the i^{th} response, respectively.

$$d_i = (y_i - L_i) / (T_i - L_i) \quad \text{Eq. 3}$$

$$d_i = (H_i - y_i) / (H_i - T_i) \quad \text{Eq. 4}$$

$$D = \left(\prod d_i^{w_i}\right)^{\frac{1}{\sum w_i}} \quad \text{Eq. 5}$$

2.1.4. Sensitivity analysis

The sensitivity of OPEX to a variation in ASR disposal and LG-MgO pricing was assessed through three different scenarios (Table 3). The baseline scenario (BASE) considers the ASR disposal and LG-MgO purchase unitary prices assumed for the multi-objective optimization (subsection 2.1.3). The Low-Price scenario (LP) assumes a well-established reuse of ASR in cement manufacturing as additive (Liang et al., 2021; Luyckx et al., 2020b; Ottosen et al., 2022), thereby eliminating the need for disposal costs (0 €/tonne).

The High-Price scenario (HP) considers a LG-MgO price of 40 €/tonne, which corresponds to the minimum cost at which the expense for $Ca(OH)_2$ and LG-MgO align, based on pilot-scale findings reported in (Boniardi et al., 2024c). All the analyses were performed through the Microsoft Excel solver tool (GRG nonlinear solving method, multi-start population size = 100). Contour plots were generated using Minitab® statistical software (distance interpolation method, power = 2).

2.2. Input data generation and collection

2.2.1. Lab-scale experiments

Experimental tests followed the methodology outlined in (Boniardi et al., 2024b), building on that study to improve the knowledge of extraction from SSA. Specifically, the present work focuses on the extraction of key metals affecting product co-precipitation (Mg, K) and contamination (Cu, Zn). Metal concentrations in the collected leachate samples were determined by microwave assisted acid digestion followed by ICP-AES analysis, in accordance with EPA 3015A 2007 and 6010D 2018 methods.

The DoE statistical approach was applied, focusing on the main leaching operating parameters discussed in literature (Meng et al., 2019; Ryszko et al., 2023; Liu et al., 2021; Fang et al., 2021; Gorazda et al., 2016; Liang et al., 2019; Luyckx et al., 2020a; Wang et al., 2018; Liu and Qu, 2016; Boniardi et al., 2021, 2022): acid type and concentration (Cn), the latter expressed as n_{eq}/L, liquid to solid ratio (L/S), expressed as $L_{acid\ solution}$/kg $_{dried\ SSA}$ and contact time (t), expressed in h. Two different designs were applied (Table 4): (i) full-factorial design (DoE#1) and (ii) extended full-factorial design (DoE#2). DoE#1 was employed for preliminary investigation of the parametric space. The design was structured with 2 levels and 4 factors, with two replicates for each test, for a total of 32 runs ($2 \bullet 2^4$). A set of axial and centre points (Cn, L/S, t = 0.2, 15, 0.5; 1, 15, 0.5; 0.6, 10, 1.25; 0.6, 15, 1.25 and 0.6, 20, 1.25) was used to validate the first-order model found. The same points were added to DoE#1 to improve the exploration of the parametric space (DoE#2), checking for any curvature within the response surface through a second-order regression model. The structure of the obtained polynomial regression models for Mg, K, Cu, and Zn extraction efficiency (EE) is shown in **Eq. (6)**:

$$EE\ (\%) = b_0 + \sum_{i=1}^{4} b_i X_i + \sum_{i,j=1, i \neq j}^{4} b_{ij} X_i X_j + \sum_{i=1}^{3} b_{ii} X_i^2 + \varepsilon \quad \text{Eq. 6}$$

where X_1, X_2, X_3 and X_4 are the factors expressed in coded units (Cn, L/S, t and acid type, respectively), b_0 is the intercept, b_i, b_{ij}, and b_{ii} are the regression coefficients for linear, interaction and quadratic terms, respectively, and ε is the random error term (residual noise). Quadratic terms were not considered for DoE#1. For both the regression models, the significance of independent variables and their interactions was tested through analysis of variance (ANOVA) at the 95% significance level ($\alpha = 0.05$). The two models were compared in terms of the goodness of extraction prediction. Whenever they provided the same accuracy, the first-order model was preferred due to the simpler interpretation of coefficients considering the physics of the extraction

Table 3
Cost scenarios in terms of ASR disposal and LG-MgO purchase costs. BASE: baseline; LP: Low-Price; HP: High-Price.

Scenario	ASR	LG-MgO
[-]	[€/tonne]	[€/tonne]
BASE	175	0
LP	0	0
HP	175	40

Table 4
Factors – acid type and concentration (Cn), liquid to solid ratio (L/S), contact time (t) – and related levels evaluated by full-factorial (DoE#1) and extended full-factorial (DoE#2) Designs of Experiments. The parametric spaces for both the Designs are graphically represented in the last row.

Factors [U.M.]	Levels	
Acid [-]	H_2SO_4 HCl	H_2SO_4 HCl
Cn [N] L/S [L/kg] t [h]	0.2–1 10–20 0.5–2	0.2–0.6–1 10–15–20 0.5–1.25–2
Design abbreviation DoE structure	DoE#1 Full-factorial	DoE#2 Extended full-factorial
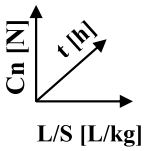	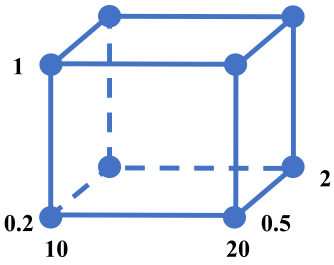	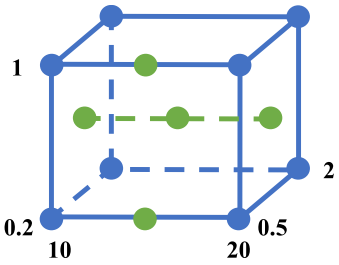

phenomena. All statistical analyses were performed using Minitab® statistical software (version 21.4.2).

The tests consisted of a preliminary mixing of the target SSA introduced in subsection 2.2.1 (7 g sample) with the acid solution, followed by centrifugation, filtration and P-PO_4^{3-} measurement. More details about the experimental procedure, including analytical methods, are provided in (Boniardi et al., 2021). The ASR from filtration were dried at 105 °C overnight by a standard lab-scale muffle furnace (Type M80-VF, MPM Instruments), estimating sol_{ash} according to **Eq. (1)**.

2.2.2. Pilot-scale experiments

Experimental tests were planned based on the leaching and precipitation operating conditions summarized in Table 5. The tests consecutively comprised wet acid leaching, coagulation, filtration, and alkaline precipitation. This sequence replicated a possible pilot-scale line of P recovery from SSA, except for the precipitate filtration, which was omitted to avoid excessive loss of the final product. More details about testing procedures and samples analyses are provided in (Boniardi et al., 2024c).

3. Results and discussion

3.1. Input data generation and literature comparison

3.1.1. Regression models for mg, K, Cu and Zn extraction efficiency

As detailed in subsection 2.2.1, the effect of acid type, Cn, L/S and t on Mg, K, Cu and Zn EE was firstly evaluated by applying DoE#1, obtaining first-order models (Table 6). DoE#1 models exhibited coefficient of determination (R^2) values higher than 0.87, highlighting a good fit to the experimental data. Pareto charts (Fig. S1, SM) and main effect plots (Figs. S2–S5, SM) indicate that an increase in Cn, L/S and t positively affected Mg, K, Cu and Zn EE, with Cn being the most influential parameter. Similar outcomes were obtained in (Fang et al., 2018a; Luyckx et al., 2020a; Liu et al., 2023). As explained in (Boniardi et al., 2024b), independently increasing these predictors enhances the diffusion phenomena through particles due to steeper H^+ concentration gradient (Cn), increased dispersion (L/S) and prolonged contact time (t). On average, H_2SO_4 was 5 and 3% more effective than HCl in extracting Mg and Zn, respectively.

Some relevant observations emerged regarding the interaction effects among parameters. Cn•t interaction plots (Figs. S2–S5, SM) indicated that t had a greater impact on Mg, K, Cu, and Zn EE when Cn was high. Specifically, a longer t could enhance the partial re-solubilization of parasitic compounds co-precipitated on ash particles, such as gypsum, thereby enhancing H^+ diffusion through ash and finally improving the extraction phenomena. Notably, high levels of Cn and t (1 N, 2 h) corresponded to the highest predicted EE for all the examined elements. Similarly, Cn•L/S interaction plots (Figs. S4 and S5, SM) revealed that Cn has a greater effect on Cu and Zn EE than L/S.

In this case, maximum Cu and Zn EE were predicted for Cn = 1 N, regardless of L/S. As reported in (Boniardi et al., 2024b), the negative coefficient for the Cn•L/S predictor could be related (i) to the ineffectiveness of increasing L/S when Cn is not high enough to extract metals or (ii) to the low relevance of increasing L/S if Cn is already sufficient to foster H^+ diffusion through particles. Finally, L/S•t interaction plots (Figs. S2 and S4, SM) indicated that as L/S increased, the significance of t on Mg and Cu EE decreased. However, high Cu EE was predicted for low L/S (10 L/kg) combined with high t (2 h).

The performance of DoE#1 models was validated at selected centre and axial points. Differences with respect to observed values ranged between −7 and −26%, with the highest variation noticed for Cu extraction by H_2SO_4 (Tables S6–S9, SM). To enhance prediction accuracy, centre and axial points were added to DoE#1 models, obtaining second-order regression models (DoE#2).

Cn remained the most influential predictor for DoE#2 models (Table 6 and Fig. S6 in SM) and the significance of the acid type on metals extraction increased compared to DoE#1 models, with H_2SO_4 being 10, 6 and 7% more effective than HCl in extracting Mg, Cu and Zn, respectively. The addition of quadratic predictors enabled the curve fitting of main and interaction plots for DoE#2 models (Figs. S7–S10, SM). Specifically, all the main effect plots for Cn exhibited an extraction peak in the range of 0.7–0.8 N, followed by a slight decrease. Similarly

Table 5
Leaching and precipitation operating conditions tested at the pilot-scale, as reported in (Boniardi et al., 2024c).

Leaching					Precipitation	
SSA	Acid	Cn	L/S	t	Precipitant type	Precipitant solution concentration
[kg]	[-]	[N]	[L/kg]	[h]	[-]	[%w/v]
5	H_2SO_4 HCl	1	10	0.5	$Ca(OH)_2$ LG-MgO	30 80

Table 6
Regression model coefficients for Mg, K, Cu and Zn EE given by the full-factorial (DoE#1) and extended full-factorial (DoE#2) Design of Experiments. Coefficients are expressed in coded units (X_1, X_2, X_3: lower level = −1; higher level = +1. X_4: H_2SO_4 = 0; HCl = 1).

DoE	DoE#1	DoE#2	DoE#1	DoE#2	DoE#1	DoE#2	DoE#1	DoE#2
Element/coefficient	Mg	Mg	K	K	Cu	Cu	Zn	Zn
b_0	61.06	73.07	27.04	34.85	43.59	63.28	32.70	49.03
b_1	11.99	11.82	9.77	10.13	14.50	15.09	9.11	9.99
b_2	9.54	9.21	4.64	4.24	6.15	4.86	4.07	3.27
b_3	4.41	4.01	3.65	3.37	5.13	–	4.36	3.94
b_4	−4.66	−10.44	–	–	–	−6.45	−2.80	−6.74
b_{12}	–	–	–	–	−4.44	−4.44	−2.35	–
b_{13}	2.98	–	2.27	1.90	4.25	–	3.80	2.91
b_{23}	−2.72	–	–	–	−3.41	–	–	–
b_{14}	3.81	–	–	–	–	–	–	–
b_{24}	–	–	–	–	–	–	–	–
b_{34}	–	–	–	–	–	–	–	–
b_{11}	–	−22.71	–	−7.53	–	−16.03	–	−7.41
b_{22}	–	–	–	–	–	–	–	−5.50
b_{33}	–	16.32	–	–	–	–	–	–
R^2	0.888	0.811	0.935	0.931	0.891	0.787	0.871	0.807
R^2_{adj}	0.856	0.786	0.926	0.923	0.865	0.764	0.840	0.776
R^2_{pred}	0.801	0.755	0.909	0.911	0.821	0.724	0.789	0.729

(Liu et al., 2023), reported that Mg, Cu and Zn EE from municipal sludge-derived hydrochar reach a plateau or a maximum for Cn ≥ 0.6 N (L/S = 10 L/kg, t = 24 h). This effect could be due to the above-mentioned parasitic co-precipitation phenomena occurring when more H^+ are available in the solution.

Except for K, the DoE#2 models provided slightly worse EE predictions than DoE#1 ones, with an average R^2 of 0.80, although they provided better prediction for the selected axial and central points (Tables S6–S9, SM). For the latter reason, these models were chosen to perform the subsequent integrated assessment of P recovery from SSA, despite the increased complexity due to the addition of quadratic predictors. However, DoE#2 models could be further improved by increasing the number of investigated points across the parametric space, i.e. by Central Composite Design (CCD).

To conclude, findings from the statistical analysis revealed that key factors for extracting Mg, K, and Zn are high levels of Cn and t, regardless of L/S. Conversely, Cu extraction was enhanced with medium Cn and high L/S levels. Low extraction of heavy metals was achieved with low Cn and low L/S (the latter only for Cu), regardless of t. Leaching by H_2SO_4 effectively enhanced Mg extraction, although it also resulted in greater Cu and Zn extractions than HCl. Therefore, the choice of the extractant should be case-specific, depending on the relative importance of maximizing nutrient content versus minimizing contaminant content. A crucial decision factor could be the minimum and maximum allowable contents of nutrients and contaminants in the recovered product, respectively.

3.1.2. Comparison between the developed predictive models and literature

DoE#1 and DoE#2 models were compared to those reported in (Luyckx et al., 2020a) for H_2SO_4 and HCl (named in the present work as DoE#LS and DoE#LH, respectively). Notably, the SSA sample accounted in (Luyckx et al., 2020a) was richer in Al (+3%) and poorer in Ca and Fe (−6% for both). Moreover, different DoE was set up (CCD with the central point replicated twice), with different ranges for the selected factors (Cn = 0.1–0.5 N, L/S = 10–50 L/kg, t = 10 min–2 h, categorical factor "acid type" was not accounted).

First, DoE#LS and DoE#LH models were applied to the experimental data from this work (Obs), as displayed in Fig. S11 in SM. Details of tested conditions are shown in Table S10 in SM. DoE#LS and DoE#LH models did not fit the experimental data as well as DoE#1 and DoE#2 models. Specifically, DoE#LS and DoE#LH underestimated the average extraction of K (−10 and −11%), Cu (−15 and −7%) and Zn (−9 and −3%) by H_2SO_4 and HCl, while overestimated that of Mg (+7 and + 10%). In particular, the worst predictions by DoE#LS and DoE#LH were noticed for Cn ≥ 0.6 N.

For completeness, DoE#1 and DoE#2 models were then applied to the experimental data reported in (Luyckx et al., 2020a) for H_2SO_4 and HCl (named in the present work as Obs#L), as displayed in Fig. S12 in SM. Tested conditions are detailed in Table S11 in SM. DoE#1 models provided a better prediction of K, Cu and Zn EE than DoE#2 models, while the latter were more effective in predicting Mg EE. On average, DoE#1 models overestimated the extraction of K (+8 and + 7%), Cu (+6 and + 5%) and Zn (+2 and + 1%) by H_2SO_4 and HCl, while DoE#2 models underestimated that of Mg (−1 and −10%).

The differences between observed and predicted values in both comparisons could be related to the distinct Cn, L/S and t ranges analysed in the two works, knowing that the reliability of a prediction can decrease when applying a regression model outside the range of the experimental conditions applied for calibration. Furthermore, the differences between DoE#1 – DoE#2 and DoE#LS – DoE#LH models could be due to the different SSA sample composition, suggesting the need to include specific predictors concerning relevant ash properties (i.e., alkalinity) to the regression models for the extraction prediction, as highlighted in (Boniardi et al., 2024b).

3.2. Multi-objective optimization

Fig. 2 displays the outcomes from the assessment on single KPIs variation in response to Cn and L/S. To be concise, only the plots corresponding to each KPIs optimal "leaching agent - precipitating agent" process configuration were included. Except for COMPL, the reference functional unit of all the KPIs (1 kg P_{rec}) depended on the selected regression model for P EE reported in (Boniardi et al., 2024b) (Ash#2, DoE#4), which did not rely on t. Therefore, the lowest t level within the analysed range (t = 0.5 h) was selected as the reference value, limiting the assessment to a two-dimensional parametric space. Conversely, COMPL was studied throughout the entire three-dimensional parametric space since the regression models for Al, Fe, Cu and Zn EE significantly depended on t, as previously discussed. To support the discussion, the contour plots of COMPL for minimum (0.5 h) and maximum (2 h) t levels were reported in Fig. 2.

Two trends can be outlined on OPEX, depending on the adopted type of extractant or precipitant. HCl-based routes exhibited lower OPEX than H_2SO_4-based ones, mainly due to the larger sol_{ash}. This effect led to a lower ASR production and, therefore, a reduced disposal cost. Similarly, LG-MgO-based routes exhibited lower costs than $Ca(OH)_2$-based ones due to the significant difference between the assumed LG-MgO (0 €/kg) and $Ca(OH)_2$ (0.12 €/kg) unitary costs. Given these observations, a

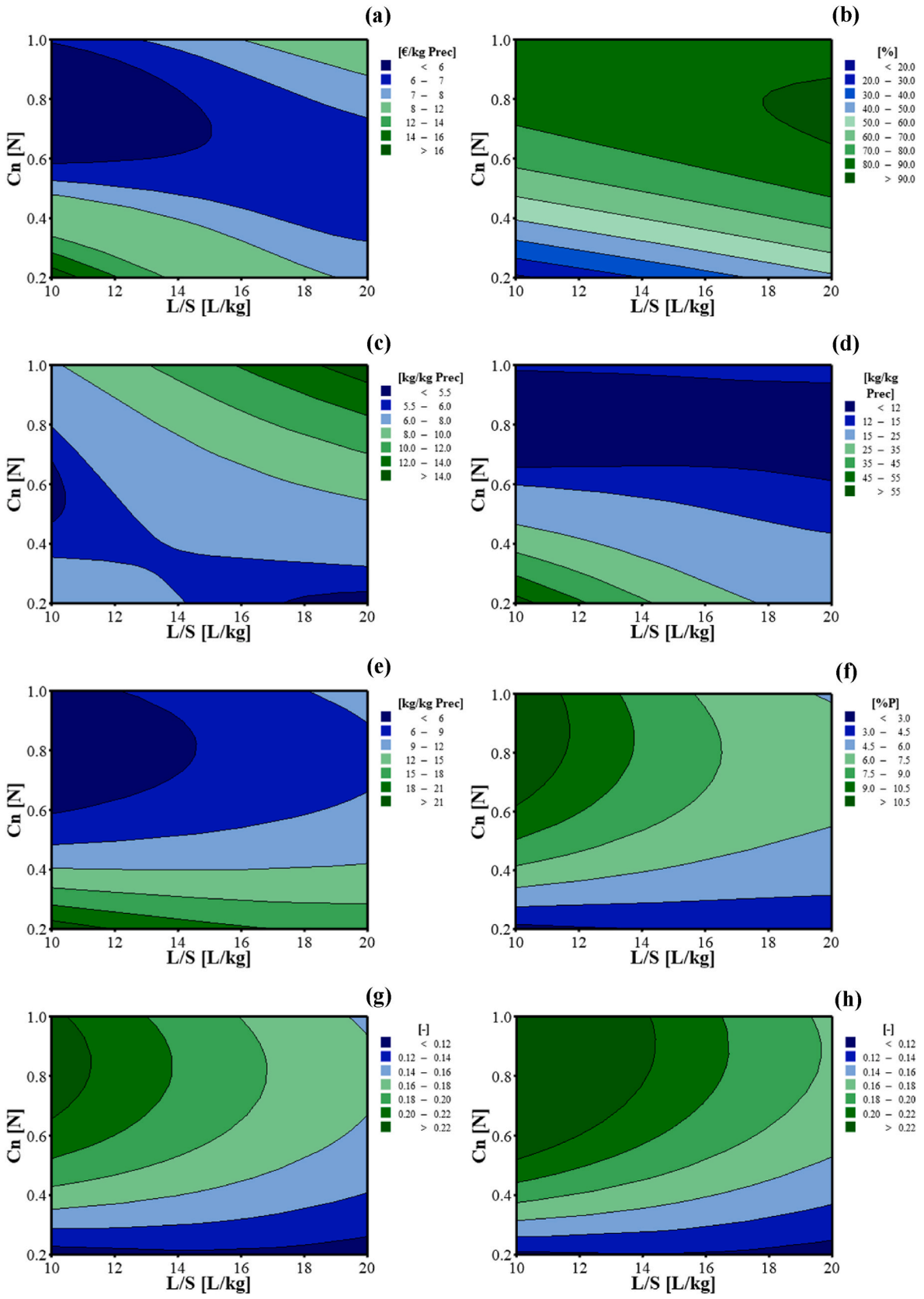

Fig. 2. Contour plots of KPIs variation with Cn and L/S. KPIs: (a) Operating Expense (OPEX); (b) Phosphorous recovery efficiency ($\eta_{recovery}$); (c) Commercial-grade acid consumption ($ACID_c$); (d) Acidic Solid Residues formation (ASR_f); (e) Dry precipitant consumption (PNT_c); (f) Phosphorous content in the precipitate ($P_{precipitate}$); (g, h): Compliance to EU 2019/1009 (COMPL). Reference t: (a–g) 0.5 h; (h) 2 h.

minimum OPEX of 5.6 €/kg P_{rec} was obtained in case of leaching by HCl (0.73 N, 10 L/kg, 0.5 h) and precipitation by LG-MgO.

P recovery efficiency ($\eta_{recovery}$) exceeded 80% for high Cn (Cn ≥ 0.8 N), regardless of L/S. This result was valid for all process configurations except for H_2SO_4 – LG-MgO, possibly due to the lower P PE observed at the pilot-scale (89%), as reported in (Boniardi et al., 2024c). Specifically, a maximum $\eta_{recovery}$ of 92% was achieved in case of leaching by HCl (0.76 N, 20 L/kg, 0.5 h) and precipitation by $Ca(OH)_2$.

H_2SO_4-based tests exhibited a lower consumption of commercial-grade acid ($ACID_c$) with respect to HCl ones, due to the greater number of equivalents per mole, which may have enhanced a reduction in the acid dose without significantly impacting P EE. Specifically, minimum $ACID_c$ of 5.1 kg/kg P_{rec} was achieved when leaching by H_2SO_4 (0.43 N, 10 L/kg, 0.5 h) and precipitating by $Ca(OH)_2$, with $Ca(OH)_2$-based routes preferred on LG-MgO-based one due to the higher levels of $\eta_{recovery}$ achieved.

HCl-based routes were characterized by lower values of ASR_f compared to H_2SO_4-based ones due to the simultaneous higher sol_{ash} and higher $\eta_{recovery}$ levels. Specifically, a minimum ASR_f of 11.7 kg/kg P_{rec} was observed in case of leaching by HCl (0.76 N, 20 L/kg, 0.5 h) and precipitation by $Ca(OH)_2$.

A minimum dry precipitant consumption (PNT_c) of 4.9 kg/kg P_{rec} was observed when leaching by HCl (0.90 N, 10 L/kg, 0.5 h) and precipitating by $Ca(OH)_2$. This configuration stood out as the best one due to the lower doses of $Ca(OH)_2$ applied at the pilot-scale compared to LG-MgO (Table S3, SM) and the higher $\eta_{recovery}$ achieved when leaching by HCl.

A maximum P content in the precipitate ($P_{precipitate}$) of 12% as P (equal to 27.5 as $\%P_2O_5$) was achieved when leaching by HCl (0.90 N, 10 L/kg, 0.5 h) and precipitating by $Ca(OH)_2$. On average, LG-MgO-based routes exhibited $P_{precipitate}$ 3% lower than $Ca(OH)_2$-based ones. This effect could be due to the higher doses of LG-MgO employed at the pilot-scale compared to $Ca(OH)_2$ (Table S3, SM), which resulted in a greater mass of the final product at the expense of $P_{precipitate}$.

The indicator expressing precipitate compliance to EU 2109/1009 (COMPL) generally increased with higher Cn and t and lower L/S. Higher Cn and t possibly enhanced the extraction of metals due to the steeper H^+ concentration gradient and the increased contact time between H^+ and ash. Conversely, augmenting L/S could have increased the leachate flow rate and, in turn, the precipitate mass (subsection 2.1.1), diluting the metal content in the precipitate. This effect might have outweighed the benefits of increased metal extraction from the enhanced dispersion.

No exceedances of Cu, Zn and Fe + Al content limits were noticed across the parametric space for any process configuration. Specifically, a minimum COMPL of 0.11 was recorded with leaching by HCl (0.20 N, 10 L/kg, 0.5 h) and precipitation by LG-MgO.

It must be specified that heavy metals regulated by EU 2019/1009 other than Cu and Zn (As, Cd, Cr, Cr (VI), Hg, Ni and Pb) were not considered in this work. Indeed, their concentrations in both lab-scale leachate and pilot-scale precipitate samples were always below the respective detection limits, preluding the calculation of their extraction and precipitation efficiencies as described in (Boniardi et al., 2021, 2024b). This outcome is consistent with findings from (Fang et al., 2018a, 2018b; Boniardi et al., 2021, 2022), which analysed SSA samples of varying origin (grate furnace and fluidized bed incineration plants) and heavy metals content, with the following concentration ranges: As (5–220 mg/kg); Cd (40–140 mg/kg); Cr (80–640 mg/kg); Hg (0.5–0.65 mg/kg); Ni (50–590 mg/kg); Pb (80–6300 mg/kg); Cu (780–1450 mg/kg); Zn (2000–14800 mg/kg). As explained in (Boniardi et al., 2021), the low content of these heavy metals in the ash often resulted in their concentrations in leachate and precipitate samples being lower than the respective detection limits, regardless of the respective EE and PE. A similar explanation could be applied to the present study, as the heavy metals content of the SSA sample analysed here is even lower (Table S1, SM). However, if significant concentrations of As, Cd, Cr, Cr (VI), Hg, Ni and Pb were detected in the leachate and precipitate, it would be necessary to estimate their EE and PE to accurately evaluate the suitability of the recovered products for fertilizer applications.

Based on previous findings, no single process configuration simultaneously optimized all the investigated KPIs. Four out of seven KPIs ($\eta_{recovery}$, ASR_f, PNT_c, and $P_{precipitate}$) were optimized when leaching by HCl and precipitating by $Ca(OH)_2$, showing similar optimal Cn levels (0.76–0.90 N) but different optimal L/S (20 L/kg for $\eta_{recovery}$ and ASR_f, 10 L/kg for PNT_c and $P_{precipitate}$). OPEX and COMPL were optimized by the same process configuration (HCl – LG-MgO) but with different Cn levels (0.73 and 0.20 N, respectively), while $ACID_c$ was minimized when leaching by H_2SO_4 (0.43 N, 10 L/kg, 0.5 h) and precipitating by $Ca(OH)_2$.

To find a compromise configuration between the investigated KPIs, the desirability method was applied. Two different composite desirability functions were developed, one excluding (D_1) and the other including (D_2) the COMPL indicator. All the KPIs were given the same importance ($w_i = 1$). Table 7 displays the optimal values for D_1 and D_2, as well as the related process configuration and KPIs values. In both cases, leaching by HCl and precipitation by $Ca(OH)_2$ appeared as the best process configuration, with slight differences in Cn levels. D_1 ensured lower values for OPEX, ASR_f and PNT_c and higher values for $\eta_{recovery}$ and $P_{precipitate}$ compared to D_2, while the latter provided lower values of $ACID_c$ and COMPL.

Both process configurations were characterized by different values for OPEX (+0.7 and + 0.6 €/kg P_{rec}), $\eta_{recovery}$ (−8 and −13%), $ACID_c$ (+6.6 and + 5.3 kg/kg P_{rec}), ASR_f (+1.1 and + 2.0 kg/kg P_{rec}) and COMPL (+0.4 and + 0.3) compared to the individual optimums. Significant variations of PNT_c (+0.4 kg/kg P_{rec}) and $P_{precipitate}$ (−1%) were observed only for D_2.

Fig. 3 displays the values of individual desirability functions (d_i) for the optimal process configurations determined by D_1 and D_2. The compromise settings were more effective in optimizing OPEX, $\eta_{recovery}$, ASR_f, PNT_c and $P_{precipitate}$ (higher d_i value) than $ACID_c$ and COMPL. This result outlined the difficulty in ensuring multi-objective optimization of the investigated P recovery process without a significant acid consumption. Specifically, achieving a trade-off between optimal recovery performances and minimum acid consumption emerged as the primary challenge in process optimization. Moreover, considering that final precipitates must comply with EU 2019/1009, regardless of how much metal concentrations fall below the limits, the COMPL indicator was neglected, thus taking D_1 as a reference configuration for process multi-optimization.

To provide additional information, the importance of KPIs was one-by-one increased to a maximum level of 10 to determine how sensitive the multi-objective solution was to the specific KPI. No relevant differences in optimal D_1 values were noticed from the analysis, with maximum variations ranging between −1% ($\eta_{recovery}$) and +5% (OPEX, $ACID_c$, ASR_f, PNT_c and $P_{precipitate}$). This finding highlighted that none of the selected KPIs had a major role in determining the compromise configuration for process multi-optimization.

3.3. Sensitivity analysis

The primary contributors to OPEX were the costs for acquiring commercial-grade acid and dry precipitant, and the expenses for disposing of ASR. The purchase costs for commercial-grade acid covered up to 35 and 65% of OPEX in case of H_2SO_4- and HCl-based process configurations, respectively, while ASR disposal contributed up to 75 and 60%. Dry precipitant cost constituted up to 25% of OPEX when using $Ca(OH)_2$. To assess OPEX sensitivity to changes in the unitary costs of processing raw materials, only the costs for dry precipitant purchase and ASR disposal were considered. The former was notably influenced by the assumption on LG-MgO unitary price, while the latter is assumed to vary significantly based on national legislation. Three cost scenarios were simulated, as introduced in Table 3, with Table 8 showing the

Table 7
Outcomes from process multi-optimization through the desirability method, excluding (D_1) and including (D_2) the KPI expressing precipitate compliance to EU 2109/1009 (COMPL).

	D	Leaching – Precipitation	OPEX	η recovery	$ACID_c$	ASR_f	PNT_c	P precipitate	COMPL
	[-]	[-]	€/kg P_{rec}	%	kg/kg P_{rec}	kg/kg P_{rec}	kg/kg P_{rec}	%P	[-]
1	0.97	HCl – $Ca(OH)_2$ (0.82 N, 10 L/kg, 0.5 h)	6.2	84%	11.7	12.8	4.9	12%	0.48
2	0.89	HCl – $Ca(OH)_2$ (0.69 N, 10 L/kg, 0.5 h)	6.2	79%	10.4	13.6	5.2	11%	0.46

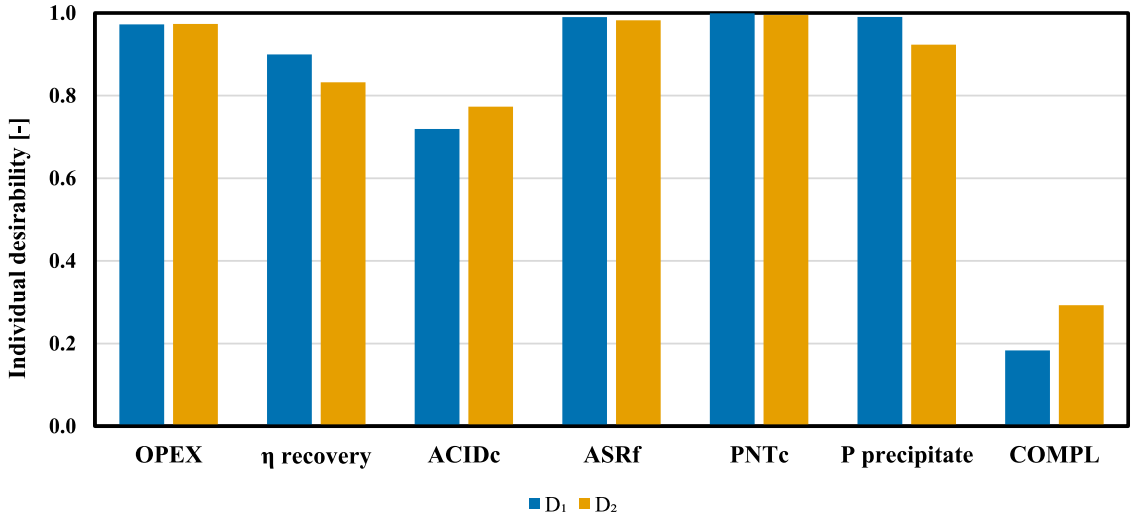

Fig. 3. Individual desirability functions for the optimal process configurations exhibited when excluding (D_1 – blue) or including (D_2 – yellow) the KPI expressing precipitate compliance to EU 2109/1009 (COMPL).

Table 8
Optimal process configurations and related OPEX for the baseline (BASE), Low-Price (LP) and High-Price (HP) economic scenarios.

Scenario	Leaching	Precipitation	OPEX
[-]	[-]	[-]	[€/kg P_{rec}]
BASE	HCl (0.73 N, 10 L/kg, 0.5 h)	LG-MgO	5.6
LP	H_2SO_4 (0.71 N, 10 L/kg, 0.5 h)	LG-MgO	2.4
HP	HCl (0.75 N, 10 L/kg, 0.5 h)	$Ca(OH)_2$, LG-MgO	6.3

corresponding optimal recovery configurations and associated OPEX levels.

Eliminating ASR disposal costs (LP) resulted in a strong decrease in the OPEX across all the process configurations, highlighting the substantial impact of ASR disposal on OPEX as previously outlined. Specifically, a minimum OPEX of 2.4 €/kg P_{rec} was identified in case of leaching by H_2SO_4 (0.71 N, 10 L/kg, 0.5 h) and precipitation by LG-MgO, possibly due to the greater impact of ASR disposal costs on the OPEX of H_2SO_4-based routes, and the assumed LG-MgO unitary cost. An increase in LG-MgO unitary price (HP) caused an increase of up to 20 and 30% in the OPEX for the H_2SO_4 – LG-MgO and HCl – LG-MgO configurations, respectively. The HP scenario exhibited a minimum OPEX of 6.3 €/kg P_{rec} when leaching by HCl (0.75 N, 10 L/kg), regardless of the precipitant used.

Data presented in Table 8 were compared to the costs outlined in (Egle et al., 2016) for 19 different P recovery technologies from wastewater treatment by-products (aqueous phases, SS and SSA). OPEX from BASE and HP scenarios were comparable to the average costs of wet chemical extraction processes from SSA, namely EcoPhos (Ohtake Tsuneda et al., 2019), Leachphos (Schaum, 2018) and PASCH (Egle et al., 2015). Instead, OPEX from LP were comparable to the average costs of thermochemical processes, namely AshDec (Canziani et al., 2023) and Thermophos (Schaum, 2018). However, it is important to note that the P recovery performances discussed in (Egle et al., 2016) were based on a reference system comprising wastewater treatment and P recovery facilities of specified capacities. Moreover, the study refers to a different historical period (2016) than the current one (2024), especially considering geopolitical concerns.

Fig. 4 displays the optimal OPEX for the three scenarios, differentiating the contributions from each cost item listed in Table S4 in SM. Across all the scenarios, the aggregate expenditure concerning energy, tap water, polyelectrolyte, maintenance, and staff were around 1 €/kg P_{rec}, with LP exhibiting the highest value for this combined cost (1.3 €/kg P_{rec}). Moreover, LP was characterized by a lower expenditure for purchasing commercial-grade acid than other scenarios. This fact could be due to the greater number of equivalents per mole related to H_2SO_4. The variation of optimal OPEX observed for HP (+0.7 €/kg P_{rec}) was notably lower than that observed for LP (−3.2 €/kg P_{rec}), underscoring the substantial impact of ASR disposal costs on this KPI. Therefore, there is a clear need to explore recovery solutions for managing this material, diverging from conventional disposal methods, to enhance the economic sustainability of the described P recovery process.

4. Conclusions

The present work introduced an innovative support tool for simulating the P recovery process from SSA. Such tool allowed to identify optimal process configurations and improvement strategies, thus promoting further attempts to guarantee the overall techno-economic

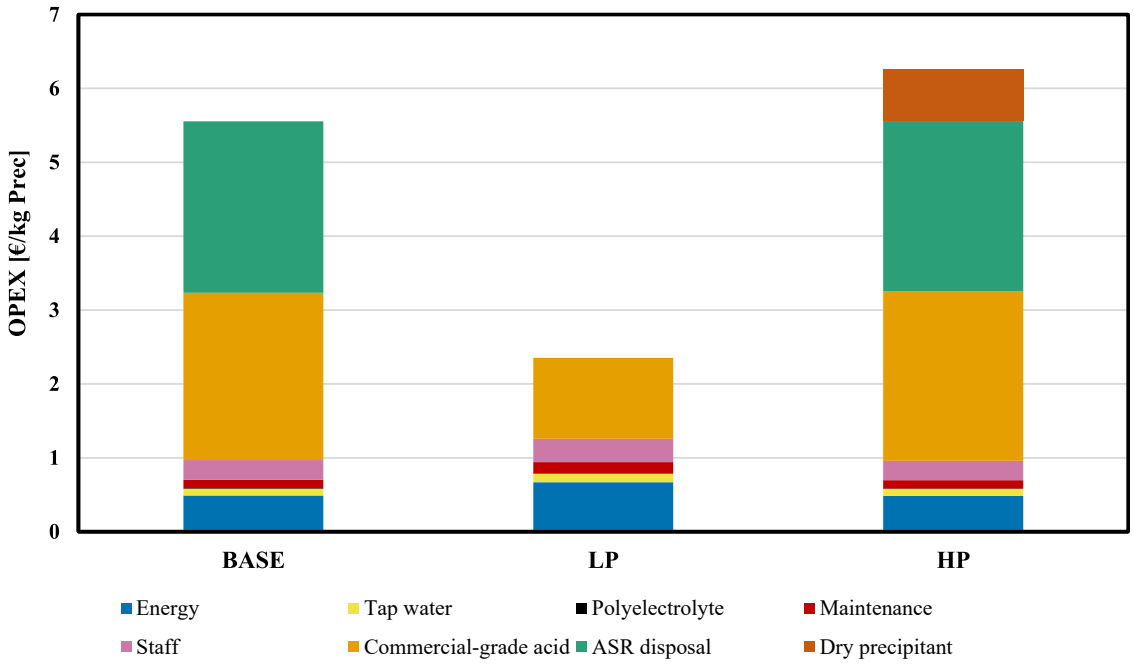

Fig. 4. Cost contributions to the optimal OPEX for the baseline (BASE), Low-Price (LP) and High-Price (HP) economic scenarios.

feasibility of the process.

Lab-scale leaching findings underscored the importance of second-order models in predicting Mg, K, Cu, and Zn extractions. Key factors for maximizing nutrient extraction (Mg, K) comprised high levels of Cn and t, while minimizing contaminants extraction (Cu, Zn) required low levels of Cn and L/S (the latter only for Cu). H_2SO_4 proved to be more effective than HCl in extracting Mg, Cu and Zn.

The process multi-objective optimization identified leaching by HCl (0.82 N, 10 L/kg, 0.5 h) and precipitation by $Ca(OH)_2$ as the optimal configuration for P recovery from SSA, despite the relevant acid consumption. Moreover, no exceedances of Cu, Zn and Fe + Al content limits were noticed.

The OPEX sensitivity analysis highlighted the relevant impact of ASR disposal costs on the overall process expenses, with OPEX ranging between 5.6 and 6.3 €/kg P_{rec} when considering this cost item or being 2.4 €/kg Prec when neglecting it. Finally, several key measures were identified to further enhance process feasibility and relevance within cleaner production framework: (i) using recycled acids and precipitants, to counterbalance high consumptions with low unitary cost, (ii) exploring recovery routes for the ASR, such as the use in cement manufacturing as additive, to abate disposal costs.

CRediT authorship contribution statement

Lorenzo Esposito: Writing – original draft, Visualization, Software, Methodology, Investigation, Formal analysis. **Gaia Boniardi:** Writing – review & editing, Supervision, Methodology, Investigation, Formal analysis, Conceptualization. **Marco Frigerio:** Resources, Investigation. **Maitane Guembe:** Investigation. **Íñigo X. García-Zubiri:** Writing – review & editing, Resources, Investigation. **Daniel El Chami:** Writing – review & editing, Resources. **Roberto Canziani:** Writing – review & editing, Resources, Conceptualization. **Andrea Turolla:** Writing – review & editing, Supervision, Project administration, Methodology, Funding acquisition, Conceptualization.

Declaration of generative AI and AI-assisted technologies in the writing process

During the preparation of this work the author used correction tools based on generative AI to improve text fluency. After using this tool, the author reviewed and edited the content as needed and takes full responsibility for the content of the publication.

Declaration of competing interest

The authors declare the following financial interests/personal relationships which may be considered as potential competing interests: Andrea Turolla reports financial support was provided by Italian Ministry of University and Research. Gaia Boniardi reports financial support was provided by Rea Dalmine. If there are other authors, they declare that they have no known competing financial interests or personal relationships that could have appeared to influence the work reported in this paper.

Acknowledgements

The research work was partially funded by the ERA-MIN3 “PHOSTER” project, co-funded by the European Union’s Horizon 2020 Research and Innovation Program, and the Italian MUR, and the Agritech National Research Center, funded by the European Union Next-Generation EU (PIANO NAZIONALE DI RIPRESA E RESILIENZA (PNRR) – MISSIONE 4 COMPONENTE 2, INVESTIMENTO 1.4 – D.D. 1032 June 17, 2022, bando CN00000022). This manuscript reflects only the authors’ views and opinions, neither the European Union nor the European Commission can be considered responsible for them.

The authors would like to thank Rea Dalmine (Greenthesis Group, Dalmine – BG, Italy) for funding the PhD grant of Ms Boniardi and providing the ash samples from the Zurich incineration plant, SEAM Engineering (Lomazzo – CO, Italy) for supporting the development of the optimization tool, Tecnoidea Impianti (Villasanta – MB, Italy) for supporting the small pilot-scale tests and Gruppo CAP (Milano – MI, Italy) for providing key data for the P recovery process integrated assessment.

Appendix A. Supplementary data

Supplementary data to this article can be found online at https://doi.org/10.1016/j.jclepro.2024.144378.

Data availability

Data will be made available on request.

References

Aguilar-Pozo, V.B., Chimenos, J.M., Elduayen-Echave, B., Olaciregui-Arizmendi, K., López, A., Gómez, J., Guembe, M., García, I., Ayesa, E., Astals, S., 2023. Struvite precipitation in wastewater treatment plants anaerobic digestion supernatants using a magnesium oxide by-product. Sci. Total Environ. 890. https://doi.org/10.1016/j.scitotenv.2023.164084.

Boniardi, G., Turolla, A., Fiameni, L., Gelmi, E., Malpei, F., Bontempi, E., Canziani, R., 2021. Assessment of a simple and replicable procedure for selective phosphorus recovery from sewage sludge ashes by wet chemical extraction and precipitation. Chemosphere 285. https://doi.org/10.1016/j.chemosphere.2021.131476.

Boniardi, G., Turolla, A., Fiameni, L., Gelmi, E., Bontempi, E., Canziani, R., 2022. Phosphorus recovery from a pilot-scale grate furnace: influencing factors beyond wet chemical leaching conditions. Water Sci. Technol. 85, 2525–2538. https://doi.org/10.2166/wst.2022.132.

Boniardi, G., Close, K., Turolla, A., Canziani, R., Oehmen, A., 2024a. Assessment of three different approaches for integrating phosphorus recovery from sewage sludge and derived products in existing wastewater treatment plants. Bioresour. Technol. 402. https://doi.org/10.1016/j.biortech.2024.130822.

Boniardi, G., Paini, E., Seljak, T., Azzellino, A., Volonterio, A., Canziani, R., Turolla, A., 2024b. Optimization of phosphorus wet acid extraction from sewage sludge ashes: detailed process insight via multi-variate statistical techniques. J. Clean. Prod. 458, 142491. https://doi.org/10.1016/J.JCLEPRO.2024.142491.

Boniardi, G., Esposito, L., Pesenti, M., Catenacci, A., Guembe, M., Garcia-Zubiri, I.X., El Chami, D., Canziani, R., Turolla, A., 2024c. Optimizing phosphorus precipitation from acidic sewage sludge ash leachate: use of Mg-rich mining by-products for enhanced nutrient recovery. J. Environ. Manag. 370, 122943. https://doi.org/10.1016/j.jenvman.2024.122943.

Canziani, R., Boniardi, G., Turolla, A., 2023. Phosphorus Recovery—Recent Developments and Case Studies, Sustainable and Circular Management of Resources and Waste towards a Green Deal, pp. 269–281. https://doi.org/10.1016/B978-0-323-95278-1.00007-3.

Desmidt, E., Ghyselbrecht, K., Zhang, Y., Pinoy, L., Van der Bruggen, B., Verstraete, W., Rabaey, K., Meesschaert, B., 2015. Global phosphorus scarcity and full-scale P-recovery techniques: a review. Crit. Rev. Environ. Sci. Technol. 45, 336–384. https://doi.org/10.1080/10643389.2013.866531.

Diego Pimenta, C., Borges Silva, M., Lima de Morais Campos, R., Ribeiro de Campos Junior, W., 2018. Desirability and design of experiments applied to the optimization of the reduction of decarburization of the process heat treatment for steel wire sae 51B35. Am. J. Theor. Appl. Stat. 7, 35–44. https://doi.org/10.11648/j.ajtas.20180701.15.

Egle, L., Rechberger, H., Zessner, M., 2015. Overview and description of technologies for recovering phosphorus from municipal wastewater. Resour. Conserv. Recycl. 105, 325–346. https://doi.org/10.1016/j.resconrec.2015.09.016.

Egle, L., Rechberger, H., Krampe, J., Zessner, M., 2016. Phosphorus recovery from municipal wastewater: an integrated comparative technological, environmental and economic assessment of P recovery technologies. Sci. Total Environ. 571, 522–542. https://doi.org/10.1016/j.scitotenv.2016.07.019.

Erro, J., Martínez-Pérez, J.M., Contreras, M.G., Márquez, R.L., García-Mina, J.M., 2023. MgO-mediated activation of active carbon as an affordable strategy to "in situ" degradation of lindane in contaminated soils. J. Environ. Manag. 344. https://doi.org/10.1016/j.jenvman.2023.118476.

ESPP. Catalogue of Nutrient Recovery Technologies, (n.d.). https://www.phosphorusplatform.eu/activities/p-recovery-technology-inventory (accessed February 21, 2024).

Fang, L., shan Li, J., Guo, M.Z., Cheeseman, C.R., Tsang, D.C.W., Donatello, S., Poon, C. S., 2018a. Phosphorus recovery and leaching of trace elements from incinerated sewage sludge ash (ISSA). Chemosphere 193, 278–287. https://doi.org/10.1016/J.CHEMOSPHERE.2017.11.023.

Fang, L., shan Li, J., Donatello, S., Cheeseman, C.R., Wang, Q., Poon, C.S., Tsang, D.C.W., 2018b. Recovery of phosphorus from incinerated sewage sludge ash by combined two-step extraction and selective precipitation. Chem. Eng. J. 348, 74–83. https://doi.org/10.1016/j.cej.2018.04.201.

Fang, L., Wang, Q., shan Li, J., Poon, C.S., Cheeseman, C.R., Donatello, S., Tsang, D.C.W., 2021. Feasibility of wet-extraction of phosphorus from incinerated sewage sludge ash (ISSA) for phosphate fertilizer production: a critical review. Crit. Rev. Environ. Sci. Technol. 51, 939–971. https://doi.org/10.1080/10643389.2020.1740545.

Gorazda, K., Tarko, B., Wzorek, Z., Nowak, A.K., Kulczycka, J., Henclik, A., 2016. Characteristic of wet method of phosphorus recovery from polish sewage sludge ash with. Open Chem. 14, 37–45. https://doi.org/10.1515/CHEM-2016-0006/MACHINEREADABLECITATION/RIS.

Gorazda, K., Tarko, B., Wzorek, Z., Kominko, H., Nowak, A.K., Kulczycka, J., Henclik, A., Smol, M., 2017. Fertilisers production from ashes after sewage sludge combustion – a strategy towards sustainable development. Environ. Res. 154, 171–180. https://doi.org/10.1016/j.envres.2017.01.002.

Gruppo CAP. Business. Water use and tariffs, (n.d.). https://www.gruppocap.it/en/services-for-citizens/our-offer/tariffs/business (accessed February 22, 2024).

Guedri, W., Mounir, J., Slah, M., 2023. Dual desirability function and RSM approaches for modeling the ideal nonwoven cover bunch for protecting date fruit. J. Text. Inst. 114, 552–561. https://doi.org/10.1080/00405000.2022.2054128.

He, P., Zhang, X., Lü, F., Shao, L., Zhang, H., 2020. Leaching behavior of phosphorous compounds from sewage sludge ash based on quantitative X-ray diffraction analysis. Waste Dispos Sustain Energy 2, 113–125. https://doi.org/10.1007/S42768-020-00037-W/FIGURES/7.

heng Fei, Y., Zhao, D., Liu, Y., Zhang, W., yuan Tang, Y., Huang, X., Wu, Q., xing Wang, Y., Xiao, T., Liu, C., 2019. Feasibility of sewage sludge derived hydrochars for agricultural application: nutrients (N, P, K) and potentially toxic elements (Zn, Cu, Pb, Ni, Cd). Chemosphere 236, 124841. https://doi.org/10.1016/J.CHEMOSPHERE.2019.124841.

IndexMundi. Triple Superphosphate Monthly Price - US Dollars per Metric Ton, (n.d.). https://www.indexmundi.com/commodities/?commodity=triple-superphosphate (accessed March 13, 2024).

IndexMundi. Rock Phosphate Monthly Price - Euro per Metric Ton, (n.d.). https://www.indexmundi.com/commodities/?commodity=rock-phosphate&months=60&currency=eur (accessed February 21, 2024).

Kootstra, A.M.J., Wim Brilman, D.W.F., Kersten, S.R.A., 2019. Dissolution of phosphate from pig manure ash using organic and mineral acids. Waste Manag. 88, 141–146. https://doi.org/10.1016/j.wasman.2019.03.038.

Li, B., Udugama, I.A., Mansouri, S.S., Yu, W., Baroutian, S., Gernaey, K.V., Young, B.R., 2019. An exploration of barriers for commercializing phosphorus recovery technologies. J. Clean. Prod. 229, 1342–1354. https://doi.org/10.1016/J.JCLEPRO.2019.05.042.

Liang, S., Chen, H., Zeng, X., Li, Z., Yu, W., Xiao, K., Hu, J., Hou, H., Liu, B., Tao, S., Yang, J., 2019. A comparison between sulfuric acid and oxalic acid leaching with subsequent purification and precipitation for phosphorus recovery from sewage sludge incineration ash. Water Res. 159, 242–251. https://doi.org/10.1016/J.WATRES.2019.05.022.

Liang, S., Yang, L., Chen, H., Yu, W., Tao, S., Yuan, S., Xiao, K., Hu, J., Hou, H., Liu, B., Yang, J., 2021. Phosphorus recovery from incinerated sewage sludge ash (ISSA) and reutilization of residues for sludge pretreated by different conditioners. Resour. Conserv. Recycl. 169. https://doi.org/10.1016/j.resconrec.2021.105524.

Liu, Y., Qu, H., 2016. Design and optimization of a reactive crystallization process for high purity phosphorus recovery from sewage sludge ash. J. Environ. Chem. Eng. 4, 2155–2162. https://doi.org/10.1016/J.JECE.2016.03.042.

Liu, H., Hu, G., Basar, I.A., Li, J., Lyczko, N., Nzihou, A., Eskicioglu, C., 2021. Phosphorus recovery from municipal sludge-derived ash and hydrochar through wet-chemical technology: a review towards sustainable waste management. Chem. Eng. J. 417. https://doi.org/10.1016/j.cej.2021.129300.

Liu, H., Lyczko, N., Nzihou, A., Eskicioglu, C., 2023. Phosphorus recovery from municipal sludge-derived hydrochar: insights into leaching mechanisms and hydroxyapatite synthesis. Water Res. 241. https://doi.org/10.1016/j.watres.2023.120138.

Luyckx, L., Van Caneghem, J., 2021. Recovery of phosphorus from sewage sludge ash: influence of incineration temperature on ash mineralogy and related phosphorus and heavy metal extraction. J. Environ. Chem. Eng. 9. https://doi.org/10.1016/j.jece.2021.106471.

Luyckx, L., Geerts, S., Van Caneghem, J., 2020a. Closing the phosphorus cycle: multi-criteria techno-economic optimization of phosphorus extraction from wastewater treatment sludge ash. Sci. Total Environ. 713, 135543. https://doi.org/10.1016/J.SCITOTENV.2019.135543.

Luyckx, L., de Leeuw, G.H.J., Van Caneghem, J., 2020b. Characterization of poultry litter ash in view of its valorization. Waste Biomass Valorization 11, 5333–5348. https://doi.org/10.1007/S12649-019-00750-6/FIGURES/7.

Meng, X., Huang, Q., Xu, J., Gao, H., Yan, J., 2019. A review of phosphorus recovery from different thermal treatment products of sewage sludge. Waste Dispos Sustain Energy 1, 99–115. https://doi.org/10.1007/s42768-019-00007-x.

Ohtake, H., Tsuneda, S., et al., 2019. Phosphorus Recovery and Recycling. Springer Singapore, Singapore. https://doi.org/10.1007/978-981-10-8031-9.

Ottosen, L.M., Thornberg, D., Cohen, Y., Stiernström, S., 2022. Utilization of acid-washed sewage sludge ash as sand or cement replacement in concrete. Resour. Conserv. Recycl. 176. https://doi.org/10.1016/j.resconrec.2021.105943.

Ryszko, U., Rusek, P., Kołodyńska, D., 2023. Quality of phosphate rocks from various deposits used in wet phosphoric acid and P-fertilizer production. Materials 16, 793. https://doi.org/10.3390/MA16020793, 793 16 (2023).

Schaum, C., 2018. Phosphorus: polluter and resource of the future - removal and recovery from wastewater. Water Intell. Online 17, 9781780408361. https://doi.org/10.2166/9781780408361.

shan Li, J., Chen, Z., ming Wang, Q., Fang, L., Xue, Q., Cheeseman, C.R., Donatello, S., Liu, L., Poon, C.S., 2018. Change in re-use value of incinerated sewage sludge ash due to chemical extraction of phosphorus. Waste Manag. 74, 404–412. https://doi.org/10.1016/j.wasman.2018.01.007.

Uzkurt Kaljunen, J., Al-Juboori, R.A., Khunjar, W., Mikola, A., Wells, G., 2022. Phosphorus recovery alternatives for sludge from chemical phosphorus removal processes – technology comparison and system limitations. Sustainable Materials and Technologies 34. https://doi.org/10.1016/j.susmat.2022.e00514.

Wang, Q., shan Li, J., Tang, P., Fang, L., Poon, C.S., 2018. Sustainable reclamation of phosphorus from incinerated sewage sludge ash as value-added struvite by chemical

extraction, purification and crystallization. J. Clean. Prod. 181, 717–725. https://doi.org/10.1016/J.JCLEPRO.2018.01.254.

Worwąg, M., 2018. Recovery of phosphorus as struvite from sewage sludge and sewage sludge ash. Desalination Water Treat. 134, 121–127. https://doi.org/10.5004/dwt.2018.22764.

Xu, Y., Zhang, L., Chen, J., Liu, T., Li, N., Xu, J., Yin, W., Li, D., Zhang, Y., Zhou, X., 2023. Phosphorus recovery from sewage sludge ash (SSA): an integrated technical, environmental and economic assessment of wet-chemical and thermochemical methods. J. Environ. Manag. 344, 118691. https://doi.org/10.1016/J.JENVMAN.2023.118691.